ACS OMEGA

Open Access

http://pubs.acs.org/journal/acsodf

Article

Optoelectronic Properties of Nitrogen-Doped Hexagonal Graphene Quantum Dots: A First-Principles Study

Published as part of ACS Omega virtual special issue "At the Speed of Light: Recent Advances in Optoelectronics".

Pham Vu Nhat, Nguyen Vo Anh Duy, Thi Nhan Tran, Nguyen Thanh Si, Truc Anh Nguyen, Nguyen To Van, Nguyen Van Nghia, Peter Schall, Van An Dinh, and Minh Triet Dang*

Cite This: *ACS Omega* 2024, 9, 20056−20065

Read Online

ACCESS | Metrics & More | Article Recommendations | Supporting Information

ABSTRACT: Graphene quantum dots have been widely studied owing to their unique optical, electrical, and optoelectrical properties for various applications in solar devices. Here, we investigate the optoelectronic properties of hexagonal and nitrogen-doped graphene quantum dots using the first-principles method. We find that doping nitrogen atoms to hexagonal graphene quantum dots results in a significant red shift toward the visible light range as compared to that of the pristine graphene quantum dots, and the doped nitrogen atoms also induce a clear signature of anisotropy of the frontier orbitals induced by the electron correlation between the doped nitrogen atoms and their adjacent carbon atoms. Moreover, time-dependent density functional theory calculations with the M06-2X functional and 6-311++G(d,p) basis set reproduce well the experimental absorption spectra reported recently. These results provide us with a novel approach for more systematic investigations on next-generation solar devices with assembled quantum dots to improve their light selectivity as well as efficiency.

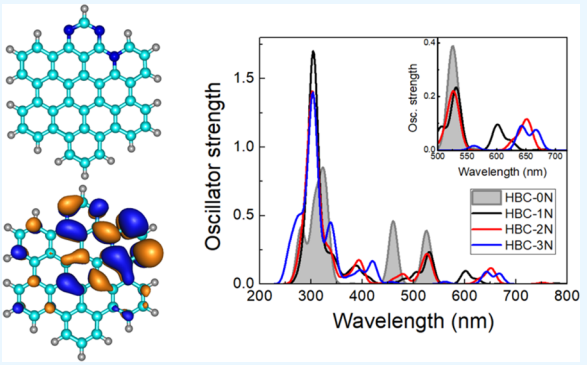

1. INTRODUCTION

Solar energy has been expected as a clean and sustainable source of energy, but the conversion of solar radiation into electric power at high efficiency remains challenging. Exploitation of interactions between nanocrystals may create an opportunity to develop new photovoltaic devices that break the Shockley−Queisser efficiency limit of solar cells.[1−3] Active control of quantum-dot superstructures allows the promotion of carrier multiplication, in which the absorption of a single photon leads to the generation of multiple electron−hole pairs to improve charge generation efficiency. Recent works[4−7] have shown the possibility to assemble semiconductor nanocrystals, and quantum dots, to investigate the interplay between nanocrystal structures, particle interactions, electronic states, and charge carrier transport for photovoltaic devices.

Graphene quantum dots (GQDs), a new kind of carbon nanoparticles that can be synthesized easily from graphene sheets via hydrothermal treatment,[8] exhibit rich optoelectronic behavior when being passivated by selective edge-functionalized groups.[9−12] These nanostructured systems have recently received major attention in engineering research due to clean, solution-processable, and biocompatible material properties.[13−16] Single-dot spectra recorded for individual carbon dots have shown that multiple active and independently excitable emission sites can exist within a single carbon dot.[17] It has been confirmed previously that such materials are able to cause a red shift in emission if they are treated by a high degree of chemical oxidation or exhibit a blue shift when being oxidized with chemical reductions or through phosphorization.[18,19] Coating graphene quantum dots on CuO/Cu to fabricate CuO/Cu/GQDs nanowire composites can enhance the electron transport kinetics of lithium-ion batteries, thanks to the decrease of the electrochemical impedance.[13] Interestingly, doping nitrogen, sulfur, and other elements can greatly enhance the optoelectronic properties of graphene quantum dots by tuning their electronic band structures.[13] Doping nitrogen atoms to the hexagonal graphene quantum dots is experimentally observed to tune their photoluminescence spectra.[17,20] The modulated photoluminescence spectra may originate from the negative induction effect of the doped heteroatoms.[21] Furthermore, the increase of the nitrogen

Received: December 29, 2023
Revised: April 11, 2024
Accepted: April 11, 2024
Published: April 24, 2024

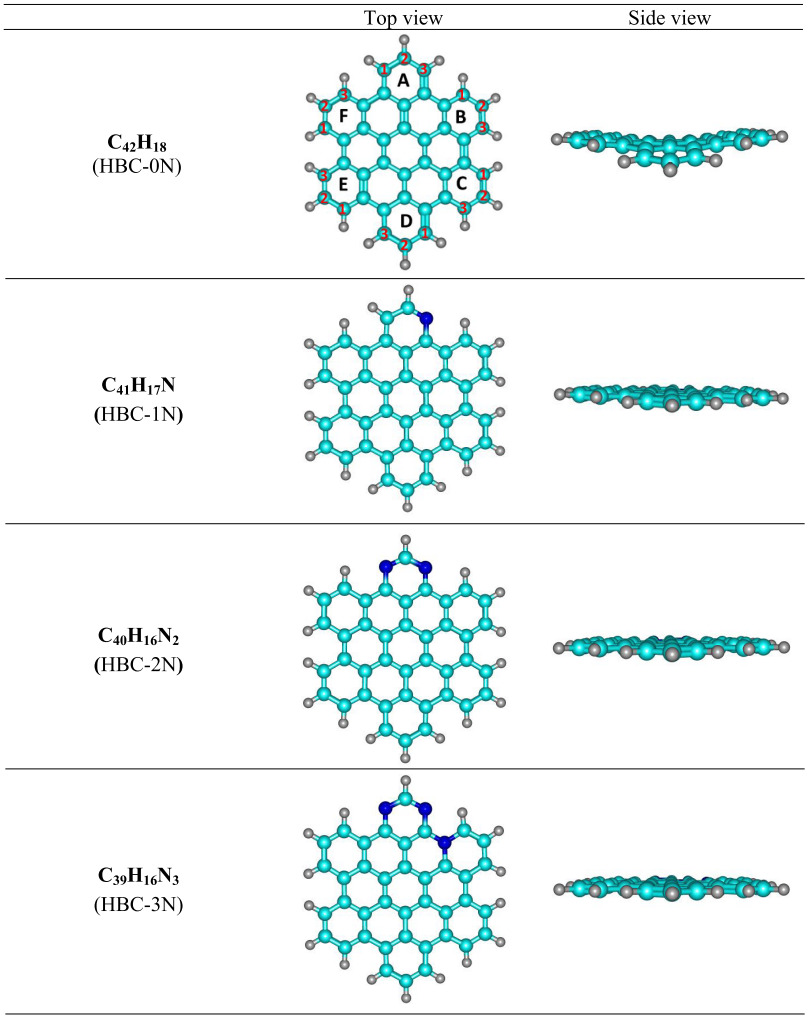

Figure 1. Equilibrium structures of nitrogen-doped graphene quantum dots at the M06-2X/6-311++G(d,p) level. The pristine graphene quantum dot (HBC-0N) also includes numbered atomic and benzene rings.

doping concentration can widen the band gaps of GQDs ranging from 2.38 to 3.79 eV,[21] resulting in high photoluminescence efficiency near-ultraviolet light-emittance. Gómez et al. pointed out that nitrogen-doped GQDs exhibit fluorescence in the entire visible region, extending to near-ultraviolet and slightly to near-infrared spectra.[22] However, theoretical insight into the underlying mechanisms when doping nitrogen to these quantum dots is lacking due to the limit of computational resources.

Additionally, graphene quantum dots also exhibit good crystallinity and rich optoelectronic behavior, and are more mechanically stable when being passivated by selective edge-functionalized groups.[9−12] Vorontsov and Tretyakov reported that for graphene dots with sizes up to 6 nm diameter, the edge formation enthalpies of armchair-edged dots without hydrogen passivation is of 13.1 eV·nm^{-1} whereas this value is only 1.3−2.7 eV eV·nm^{-1} for hydrogen passivated edges, indicating that hydrogen edge passivation can assist structural stability of the graphene dots.[23]

In this context, we set up a theoretical study to thoroughly examine the effect of doped nitrogen atoms on optoelectronic properties of hexagonal graphene quantum dots in a vacuum using density functional theory (DFT) simulations.[24−29] In particular, we clarify the modifications in structures, frontier energy levels, projected density of states (DOS), and optical absorption of quantum dots in the presence of foreign atoms. We find that doping nitrogen atoms to hexagonal graphene quantum dots, the optical absorption experiences a strong expansion of the visible spectrum covering from the purple to the red light ranges, and the ultraviolet absorption efficiency is considerably enhanced as compared to that of the pristine graphene quantum dots. These results open new opportunities to tune graphene quantum dots toward applications in solar cell devices.

2. COMPUTATIONAL DETAILS

From the typical two-dimensional graphene structure, we cut the graphene sheet into smaller hexagonal graphene quantum dots and passivated these dots with hydrogen atoms. We then perform geometrical optimization of ground states on these newly obtained graphene quantum dots using the DFT method implemented in the Gaussian 16 package.[30] For the frontier orbital energy gaps and excitation energy predictions, we employ multiple exchange−correlation functions across the Jacob's Ladder[31] including the range-separated LC-BLYP[32−34] and the LC-ωPBE, hybrid-meta-generalized gradient approximations (hybrid-meta-GGA) M06-2X[35] and the GGA Perdew−Burke−Ernzerhof (GGA PBE) exchange−correlation functionals[36] with a 6-311++G(d,p) basis set. Note that while

https://doi.org/10.1021/acsomega.3c10501
ACS Omega 2024, 9, 20056−20065

Table 1. Formation Energy E_f, Gibbs Energy ΔG, and Diameters of Nitrogen-Doped Graphene Quantum Dots[a]

	formation energy (eV)			ΔG (eV)			diameter (Å)		
samples	range-separated	hybrid-meta-GGA	GGA	range-separated	hybrid-meta-GGA	GGA	range-separated	hybrid-meta-GGA	GGA
HBC-0N							13.426/13.507	13.491	13.587
HBC-1N	4.8/4.8	5.0	4.9	4.3/4.0	4.4	4.4	13.747/13.523	13.546	13.619
HBC-2N	9.7/9.8	10.0	9.7	8.6/8.4	8.9	8.6	13.466/13.516	13.537	13.606
HBC-3N	10.6/10.9	11.1	11.2	9.6/9.6	10.1	10.2	13.378/13.428	13.466	13.556

[a]DFT exchange−correlation functionals include range-separated (LC-BLYP/LC-ωPBE, respectively), hybrid-meta-GGA (M06-2X) and GGA (PBE).

the long-range LC-BLYP exchange functional has sufficiently improved the calculated orbital energies in noble clusters,[26,27,37] M06-2X with double the amount of nonlocal exchange may yield better agreement to the experimental optical responses of graphene quantum dots. We further employ the same basis sets to calculate excitation energies by the time-dependent DFT (TD-DFT) method. The convergence criteria are set at 3×10^{-4} au for the root-mean-square (RMS) of force and at 4.5×10^{-4} au for the maximum force. For the TD-DFT method, we take into account at least the first 120 lowest excited states (singlet:triplet = 1:1). To calculate the electronic density of states (DOS), we record the TD-DFT molecular orbitals of the optimized geometries in the singlet states and use the GaussSum program[38] to calculate group contributions to molecular orbitals and convoluted these Gaussian curves by a full width at half maximum (fwhm) of 0.3 eV.

To evaluate the stability of the nitrogen-doped GQDs, we define the formation energy (E_f) as follows:[39]

$$E_f = E(C_{m'}H_nN) - E(C_mH_n) - \mu_N - (m' - m)\mu_C \quad (1)$$

where $E(C_mH_n)$ and $E(C_{m'})H_nN$ are the total electronic energies of pristine and nitrogen-doped GQDs, while μ_C and μ_N are the chemical potentials of carbon and hydrogen atoms, respectively. The indices m (m') and n (n') are the number of carbon and hydrogen atoms in the GQDs.

Using a similar approach, we also define the enthalpy and Gibbs free energy of the interactions using the following expressions:

$$\Delta H = H(C_{m'}H_nN) - H(C_mH_n) - H_N - (m' - m)H_C \quad (2)$$

$$\Delta G = G(C_{m'}H_nN) - G(C_mH_n) - G_N - (m' - m)G_C \quad (3)$$

where H is the sum of the electronic and thermal enthalpies and G is the sum of the electronic and thermal free energies.[40]

3. RESULTS AND DISCUSSION

3.1. Geometrical Structures. To study the optoelectronic properties of nitrogen-doped graphene quantum dots, we first optimize the geometrical structures of these quantum dots to obtain the most stable configurations. For convenience, the GQDs with numbered benzene rings (from A to F) and bound carbon atoms of each ring (numbered from 1 to 3) are depicted in Figure 1. Experimentally, the doping atoms are energetically favorable to sit at the edges replacing the bounding carbon atoms and functional groups.[41] Thus, in this study, we replace the carbon atoms with nitrogen atoms in only these regions. Thanks to the perfect symmetrical characteristic of the quantum dot, we replace the boundary carbon atoms at positions 1, 2, and 3 of the benzene rings with a nitrogen atom. The nitrogen-doped structures, abbreviated as HBC-xN where x is equal to 0, 1, 2, and 3 nitrogen atoms, are formed by replacing a boundary carbon atom in the original hexa-peri-hexabenzocoronene (HBC) structure.[42] In the HBC-1N structure, a substituted carbon atom can be placed at either the A_1 or A_2 position (Figure 1). The HBC-2N samples were developed by further replacing the C atom at the boundaries of the HBC-1N stable configuration. The HBC-3N then is formed in a similar procedure. Details of these structures are presented in the Supporting Information section. Here, we introduce only stable structures of HBC-xN with x = 0, 1, 2, and 3. Note that in this study, we assume that the most favorable doping positions are at the boundary since the most stable HBC-1N is obtained by substituting a carbon atom and a nitrogen atom at the boundary. Thus, for HBC-2N and HBC-3N, the potential substitutional sites are evaluated only for the outer rings. A more robust approach is to perform molecular dynamics simulations to evaluate all possible configurations.

Figure 1 illustrates the optimal structures of the differently doped GQDs obtained with functional M06-2X/6-311++G(d,p). Similar geometrical optimization strategies are applied by various exchange−correlation functionals including LC-BLYP, LC-ωPBE, and PBE. Table 1 presents the values of the formation energy E_f, Gibbs energy ΔG, and diameters of HBC-xN, defined as the distance between the two furthest carbon atoms of the HBC-xN quantum dots. It is obvious that the absolute quantities of formation energies and Gibbs energies of HBC-1N are much smaller than HBC-2N and HBC-3N, indicating that HBC-1N is energetically more stable than others. These observations still hold for the other investigated functionals, indicating that this finding is robust. In terms of molecular bond lengths, we notice a moderate reduction of carbon−carbon bond lengths after hydrogenation: the outer edges of the quantum dots reduce from a regular bond length of 1.445 Å inside the GQDs to either 1.379 or 1.400 Å at the outer edges. The carbon−hydrogen bonds are of length 1.081 Å. Thus, hydrogenation leads to a decrease of carbon−carbon bond lengths in the armchair edge, and this observed compactness is in line with the calculations obtained by the PM7 semiempirical method.[23]

Furthermore, the large formation energies of all nitrogen-doped GQDs in Table 1 also indicate that they are energetically less stable than their pristine counterparts. These large formation energies also imply the difficulty of synthesizing nitrogen-doped GQDs. In fact, as reported in ref 21, these dots can be obtained by heating up nitrogenous "graphite" compounds up to 800−1200 °C under 4.0 GPa for 72 h. Among all possible adsorption sites, HBC-1N turns out as the most stable configuration with the smallest (positive) formation energy and Gibbs energy with respect to HBC-2N and HBC-3N structures: the more the number of nitrogen

https://doi.org/10.1021/acsomega.3c10501
ACS Omega 2024, 9, 20056−20065

atoms doped into the quantum dots, the higher the formation energy and Gibbs free energy cost of these dots. More interestingly, the fact that the Gibbs free energy is smaller than the formation energy emphasizes the role of entropic effects upon adsorption: mixing nitrogen atoms into the graphene lattice increases the entropy; thus, the presence of nitrogen atoms increases disordering, resulting in higher entropy and lower Gibbs free energy.[43]

3.2. Vibrational Analyses. Analysis of vibrational features plays an essential role in the rationalization of the absorption mechanism, and the infrared spectra can shed light on experimental studies to detect typical vibrational modes of molecules. Figure 2 and Table 2 present in detail the vibrational spectra of pristine and nitrogen-doped GQDs. The IR spectra of the pristine dots exhibit dominant intensity peaks at around 785 cm^{-1} corresponding to the out-of-plane modes of C═C−H bond deformation. This typical peak was reported theoretically in ref 44. and experimentally in ref 45. We also detect the in-plane bending mode of C═C−C groups from the weaker peaks at around 823 cm^{-1} and the C═C bond stretching mode at 1622 cm^{-1}, in excellent agreement with the recent measurement for carbon dots.[20] The vibrational C−H bonds are computed at ∼3215 and 3254 cm^{-1}.

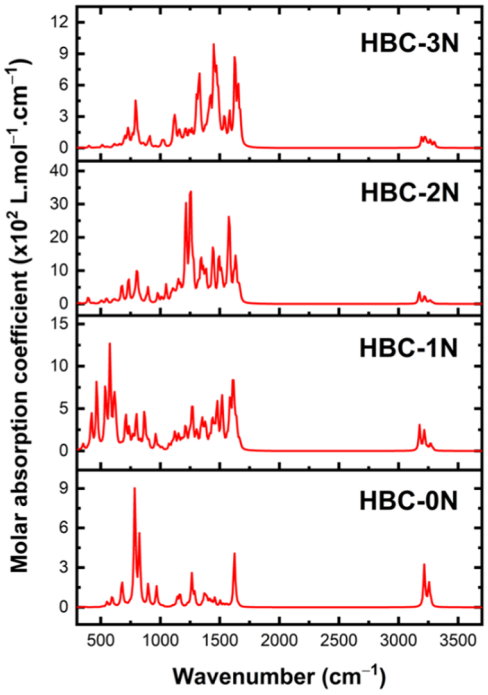

Figure 2. Infrared spectra of nitrogen-doped GDQs at the M06-2X/6-311++G(d,p) level.

In the nitrogen-doped graphene quantum dots, new vibrational modes induced by the adsorbed nitrogen atom are detected. The IR spectra of HBC-1N show a sharp peak at 1634 cm^{-1} representing the stretching mode of the C═N bond. This C═N stretching vibration is experimentally detected at 1668 cm^{-1} from Fourier transform infrared (FT-IR) spectra of carbon dots.[20] The stretching modes of C−H bonds remain almost unchanged at 3175−3268 cm^{-1} in HBC-1N compared to 3215−3254 cm^{-1} of the equivalent pristine HBC-0N GQDs. The absorption peaks at 800 and 1270 cm^{-1} are attributed to the in-plane bending of C═C−H and C−H bonds, respectively.

In the case of HBC-2N and HBC-3N GQDs, the IR spectra are almost similar. The peak positions of discernible signals do not alter much; however, the peak intensities of the larger GQDs reduce noticeably. This demonstrates that upon increasing the number of nitrogen-doped atoms, the out-of-plane bending of C−H bonds at 1212 (HBC-2N) and 1330 cm^{-1} (HBC-3N) and the symmetric stretching of the C═C and C═N bonds at 1574, 1583 (for HBC-2N) and 1581 and 1627 cm^{-1} (for HBC-3N) still play a dominant role in the vibrational modes of these dots. However, since the vibrational mode of C−H bonds becomes weaker, the peak intensities are less pronounced. This explains the broad absorption bands from 3000 to 3500 cm^{-1} reported in the experimental FT-IR spectra of GQDs.[46] The in-plane bending of C═C bonds at 1574 cm^{-1} for HBC-2N becomes more prominent, pointing out the high possibility to be measured. This vibrational mode was observed at 1570 cm^{-1} in the FT-IR spectra when cutting a graphene sheet into nanometer-size GQDs.[8]

3.3. Electronic Properties. Nitrogen has an electronegativity of 3.04, which is significantly higher than that of carbon with 2.55. Therefore, the doped nitrogen atoms attract shared electrons from their adjacent carbon atoms. The correlation between the doped nitrogen atoms and the carbon atoms is predicted to tune not only the vibrational features but also the optical properties of the GQDs. To obtain deep insights into the effect of a nitrogen-doped atom on the optical properties of GQDs, we examine the energies of frontier orbitals [the highest occupied molecular orbital (HOMO) and the lowest unoccupied molecular orbital (LUMO)], HOMO−LUMO band gap (E_g). As listed in Table 3, the band gap

Table 2. Selected IR Band Positions (in Unit of cm^{-1}) and Molar Absorption Coefficient (in Unit of $L{\cdot}mol^{-1}{\cdot}cm^{-1}$) Computed for Nitrogen-Doped GDQs at the M06-2X/6-311++G(d,p) Level[45a,b]

	HBC-0N		HBC-1N		HBC-2N		HBC-3N	
	position	intensity	position	intensity	position	intensity	position	intensity
γ(C═C−H)	785	903	800	437	805	960	793	454
β(C═C−C)	823	561	866	460	896	517	910	114
β(C−H)	1264	262	1270	525	1212	2400	1330	700
ν(C═C)	1622	400	1611	836	1574	2614	1581	360
ν(C ═ N)			1634	430	1583	2296	1627	869
ν_{as}(C−H)	3215	325	3218	250	3224	213	3220	106
ν_{s}(C−H)	3254	324	3175−3268	88−310	3173−3269	100−353	3193−3299	56−106

[a]The experimental γ(C═C−H) IR mode in an Argon matrix is 772 cm^{-1}.[45] [b]ν_s, symmetric stretching, ν_{as}, asymmetric stretching, β, in-plane bending, γ, out-of-plane deformation.

https://doi.org/10.1021/acsomega.3c10501
ACS Omega 2024, 9, 20056−20065

Table 3. Energies (eV) of HOMO, LUMO Frontier Orbitals and HOMO−LUMO Band gap (E_g) of Pristine and Nitrogen-Doped GDQs[a]

	range-separated			hybrid-meta-GGA			GGA		
samples	HOMO (eV)	LUMO (eV)	E_g (eV)	HOMO (eV)	LUMO (eV)	E_g (eV)	HOMO (eV)	LUMO (eV)	E_g (eV)
HBC-0N	−5.37/−5.44	−0.13/−0.24	5.24/5.19	-4.10	−1.54	2.55	−3.08	−2.84	0.24
HBC-1N	−5.95/−6.01	−0.51/−0.65	5.44/5.36	-4.40	−1.83	2.57	−3.24	−2.96	0.27
HBC-2N	−6.07/−6.13	−0.70/−0.84	5.37/5.29	-4.58	−1.96	2.62	−3.36	−3.11	0.25
HBC-3N	−6.42/−6.42	−0.40/−0.56	6.02/5.85	-5.03	−1.74	3.29	−3.73	−2.98	0.76

[a]DFT exchange−correlation functionals include range-separated (LC-BLYP/LC-ωPBE, respectively), hybrid-meta-GGA (M06-2X) and GGA (PBE).

energies of HBC-0N are 5.24, 5.19, 2.55, and 0.24 eV from the LC-BLYP, LC-ωPBE, M06-2X/6-311++G(d,p), and PBE functionals, respectively. Note that to predict orbital energies of molecular clusters, the range-separated and hybrid-meta-GGA functionals are more reliable than the PBE functional.[26,47−50] The calculations by five functionals show that, in the presence of nitrogen-doped atoms, the electronic gap of GQDs is broadened, and the increase of the band gap is proportional to the nitrogen-doped concentration as exhibited in Figure 3. The band gaps of HBC-1N, HBC-1N, and HBC-3N computed by M06-2X/6-311++G(d,p) theoretical model are respectively 2.57, 2.62, and 3.26 eV, which also exhibit a better agreement with experimental data.[26,47−51] It means that the M06-2X/6-311++G(d,p) functional coves well the intrinsic electronic interaction of the considered nitrogen-doped GQD samples, and therefore, it is trusted to use the M06-2X/6-311++G(d,p) functional to further explore the effect of doping nitrogen on optoelectronic properties of GQDs.

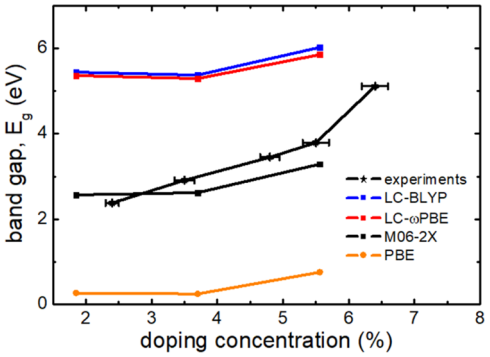

Figure 3. Band gap versus doping nitrogen concentrations of graphene quantum dots. The experimental values were obtained from ref 21. The HOMO−LUMO band gap values were obtained from the range-separated (LC-BLYP/LC-ωPBE, respectively), hybrid-meta-GGA (M06-2X) and GGA (PBE) functionals at the 6-311++G(d,p) level.

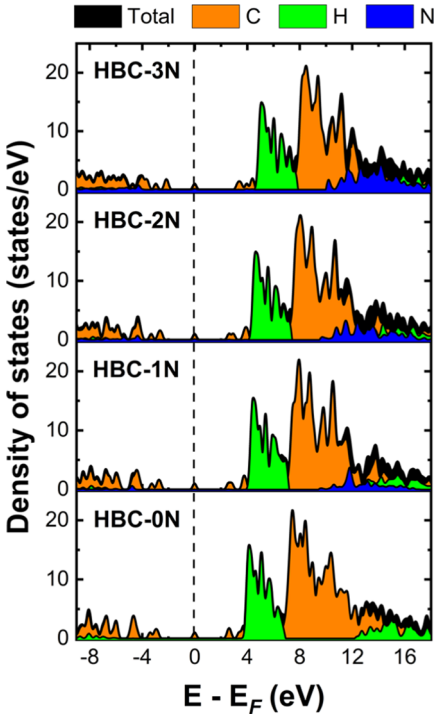

Figure 4. Partial density of states of $C_{42-x}H_{18-x}N_x$ graphene quantum dots obtained from the M06-2X functional. x is the number of nitrogen atoms in the quantum dots. The Fermi level is indicated as a vertical black dashed line.

The broadening of the electronic gap can be further confirmed by the analysis of the partial density of states (DOS) of nitrogen-doped GQDs. Figure 4 presents the partial DOS of $C_{42-x}H_{18-x}N_x$ GQDs (x is the number of nitrogen atoms in the quantum dots, varying from 1 to 3) obtained by the M06-2X/6-311++G(d,p) functional. It is obvious that the HOMO and the LUMO of GQDs with and without doped nitrogen atoms are occupied by electrons of the carbon atoms. Moreover, there is a strong downshift of the HOMO toward the second occupation molecular orbital (SOMO) in the valence band, reducing the separation between the HOMO and the SOMO. The downshift of the HOMO is consistent with the enlargement of the electronic gap induced by the doping of nitrogen atoms indicated above. To gain further insight into the effect of nitrogen doping on the optoelectronic properties of GQDs, we analyze the HOMO and LUMO shapes of the most stable pristine GQD and nitrogen-doped GDQs in Figure 5. For pristine GQDs, the HOMO and LUMO schemes exhibit a high geometric symmetric distribution on the surface. However, the attraction of shared electrons of the adjacent carbon atoms leads to the redistribution of electrons of the frontier orbitals on the surfaces of GQDs, breaking the symmetry of the HOMO and LUMO shapes. The carbon atoms adjacent to the doped nitrogen atoms acquire a higher positive charge than others. For the LUMO states of nitrogen-doped GQDs, there is an additional appearance of electron depletion and accumulation regions located around the center of the GQDs. Especially, the HOMO scheme of nitrogen-doped GQDs exhibits a stronger modification than the LUMO shapes, meaning that the energy shift caused by doping nitrogen atoms of the HOMO is stronger than that of the LUMO shown in Table 3. In addition, the change of the HOMO form is highly sensitive to the

https://doi.org/10.1021/acsomega.3c10501
ACS Omega 2024, 9, 20056−20065

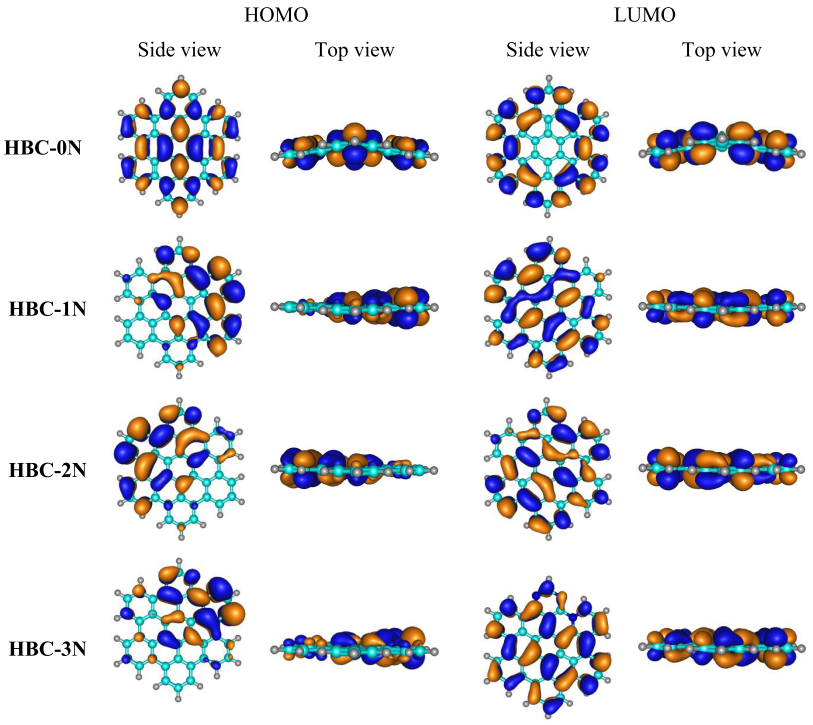

Figure 5. Shapes of frontier orbitals of the most stable nitrogen-doped GDQs at the M06-2X/6-311++G(d,p) level. Isovalue for the orbital rendering is 0.02 eV/Å^2. The electron depletion is in blue whereas the electron accumulation is in reddish brown.

number of doped nitrogen atoms. Compared to the pristine GQDs, the change of the LUMO scheme of the HBC-3N structure is the greatest, in line with the largest broadening of its band gap indicated above. Furthermore, as shown in Table S3, upon increasing the nitrogen doping concentration, the number of sigma bonds increases. In other words, the π cloud density decreases, leading to band gap opening. These results again emphasize the role of a negative induction effect upon nitrogen doping to graphene quantum dots.

3.4. Optical Responses. It is known that density functional theory may under- or overestimate the band gap as well as the absolute values of the optical absorption spectra of investigated materials. Choosing the appropriate exchange−correlation functions is crucial for predicting these quantities. Thanks to the perfect match between the predicted band gaps and the experimental results in the previous section, we perform optical absorption calculations using the M06-2X/6-311++G(d,p) method. Figures 6 and 7 present the absorption spectra and the shapes of frontier orbitals associated with the dominant absorption peaks, which quantitatively prove the electronic origin of these absorption spectra.

In the ultraviolet range, the dominant absorption peak of the HBC-0N is centered at 324 nm, which is in excellent agreement with the experimental observation for HBC at 363 nm.[18] This peak is assigned to the $\pi-\pi^*$ transition from HOMO − 1 to LUMO + 1. The second noticeable peak in this region appears at 280 nm, originating from the electron transition from HOMO − 3 to LUMO. Upon doping nitrogen atoms to the GQDs, we observe a considerable modification of the absorption spectra both in the ultraviolet and visible light ranges. In the presence of a nitrogen atom in the graphene dot, the dominant peak intensity at 306 nm, which is mainly contributed by the charge transfer from LUMO + 1 to HOMO − 1, is double the dominant peak of the parent structure. In the case of the HBC-2N and HBC-3N structures, we observe

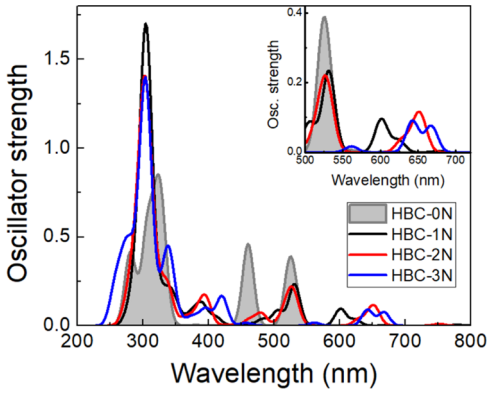

Figure 6. Absorption spectra of nitrogen-doped GDQs at the M06-2X/6-311++G(d,p) level.

dominant absorption peaks at 302 and 304 nm induced by the charge transfer from LUMO + 1 to HOMO − 2 and from LUMO to HOMO − 2, respectively. These two peaks are remarkably more pronounced than that of the highest-intensity peak of HBC-0N. In short, the doping of nitrogen enhances remarkably the absorption efficiency of GQDs to photons in the ultraviolet region.

In the visible light range, pristine GQDs are highly sensitive to photons in a narrow range from 430 to 550 nm with two intense absorption peaks centered at 460 and 526 nm. However, by doping nitrogen atoms with GQDs, we observe a wider absorption spectrum with many more distinct absorption peaks in this region. For instance, in the case of the HBC-1N sample, as shown in Table 4, we can observe three pronounced peaks at 388, 530, and 602 nm, resulting from the electron transitions from LUMO + 7 to HOMO, LUMO + 3 to HOMO, and LUMO + 2 to HOMO, respectively. For the HBC-2N structure, the calculations

https://doi.org/10.1021/acsomega.3c10501
ACS Omega 2024, 9, 20056−20065

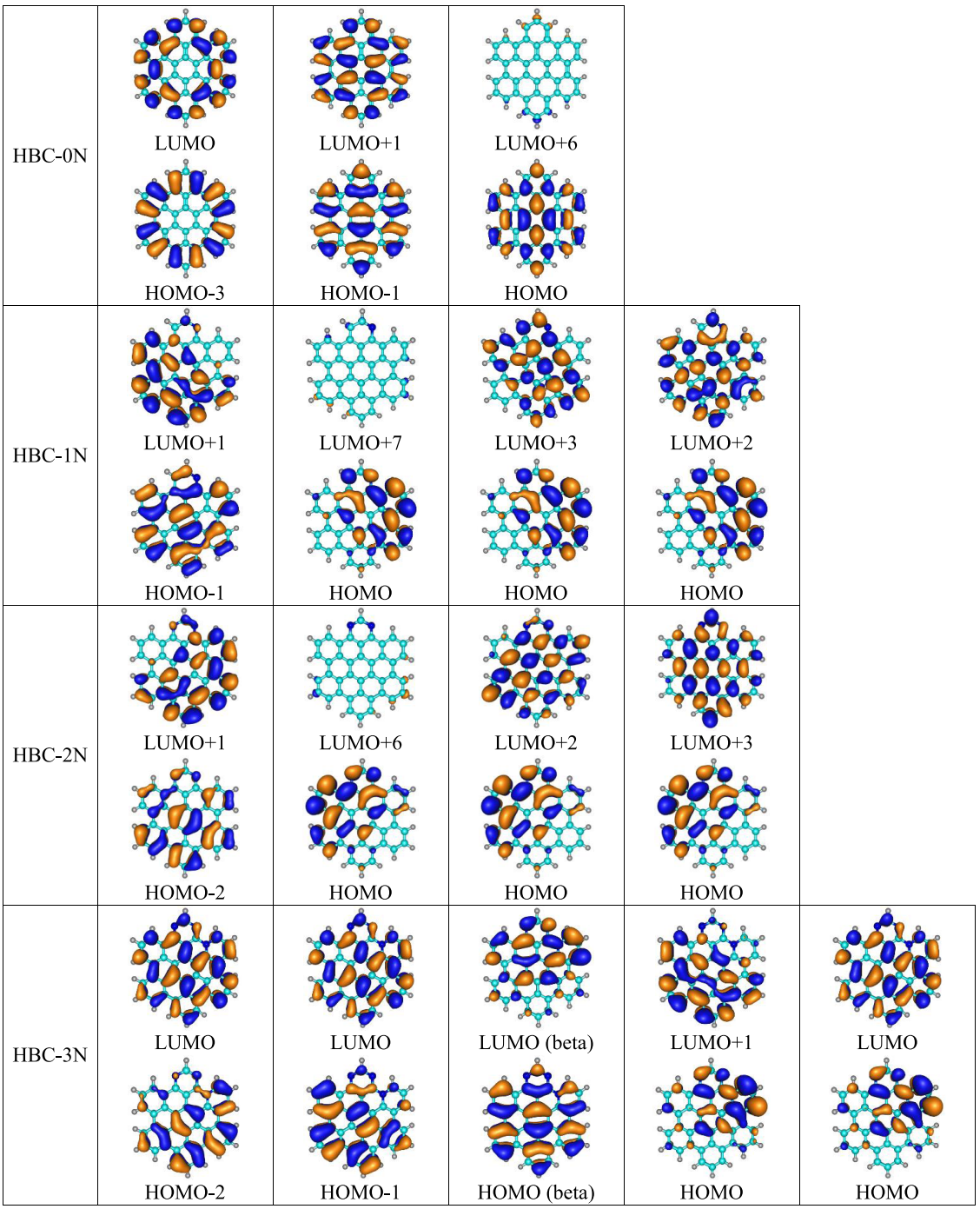

Figure 7. Shapes of frontier orbitals associated with the dominated absorption peaks presented in Figure 6 at the M06-2X/6-311++G(d,p) level.

predict three intense peaks at 392, 526, and 650 nm, corresponding to the transitions from LUMO + 6 to HOMO, LUMO + 2 to HOMO, and LUMO + 3 to HOMO, respectively. For HBC-3N, the intense absorption peaks are located at 420, 642, and 666 nm, which mostly originate from the transition of LUMO in the β orbital to HOMO, LUMO + 1 to HOMO, and LUMO to HOMO, respectively. The red shift of the absorption spectrum upon increasing the number of nitrogen-doped atoms is in quantitative agreement with experimental observations reported in ref 21. These results demonstrate the essence of orbital interactions upon doping nitrogen atoms with graphene dots to enhance the energy conversion efficiency of solar cell panels embedded by these dots.

4. CONCLUDING REMARKS

In this study, first-principles approaches have been employed to elucidate the optoelectronic properties of both pristine and nitrogen-doped hexagonal graphene quantum dots. Though doping nitrogen atoms to these dots requires additional energy cost to stabilize the resulting products, this is an effective way to improve the optoelectronic properties of quantum dots. We observed for the first time a considerable modification of the frontier orbitals induced by the electron correlation between the doped nitrogen atoms and their adjacent carbon atoms. By

https://doi.org/10.1021/acsomega.3c10501
ACS Omega 2024, 9, 20056−20065

Table 4. Wavelength/Energy (nm/eV) and Oscillator Strength (f) of Intense Absorption Peaks in the UV−vis Region of Pristine and Nitrogen-Doped GQDs at the M06-2X/6-311++G(d,p) Level

	wavelength/energy (nm/eV)	transitions	f
HBC-0N	280/4.83	HOMO − 3 → LUMO	0.41364
	324/3.83	HOMO − 1 → LUMO + 1	0.85091
	460/2.70	HOMO → LUMO + 6	0.46016
	526/2.36	HOMO → LUMO + 6	0.38930
HBC-1N	306/4.05	HOMO − 1 → LUMO + 1	1.70084
	388/3.20	HOMO → LUMO + 7	0.13622
	530/2.34	HOMO → LUMO + 3	0.23373
	602/2.06	HOMO → LUMO + 2	0.09665
HBC-2N	302/4.11	HOMO − 2 → LUMO + 1	1.40537
	392/3.16	HOMO → LUMO + 6	0.17440
	526/2.36	HOMO → LUMO + 2	0.22144
	650/1.91	HOMO → LUMO + 3	0.11602
HBC-3N	304/4.08	HOMO − 2 → LUMO	1.39919
	338/3.67	HOMO − 1 → LUMO	0.45149
	420/2.95	HOMO → LUMO[a]	0.16905
	642/1.93	HOMO → LUMO + 1	0.09157
	666/1.86	HOMO → LUMO	0.07698

[a]This contribution is β orbitals.

evaluating several hybrid exchange−correlation functions are evaluated, the M06-2X functional combined with the 6-311++G(d,p) basis set is strongly suggested to predict the absorption spectra of such quantum dots. It perfectly reproduces the clear red shift of the absorption spectra with increasing number of doped nitrogen atoms as experimentally observed.[21] The calculated absorption spectra consist of several novel absorption peaks with significant intensity enhancement, leading to an improvement in light-to-electricity energy conversion efficiency. Furthermore, upon increasing the nitrogen doping concentration, the band gap opening is induced by the increase in sigma bonds between the substitutional nitrogen atoms and carbon atoms, nicely illustrating the negative induction effect of nitrogen atoms on graphene quantum dots. These results pave a novel way for the design of tunable electrical and photonic devices based on graphene quantum dots.

■ ASSOCIATED CONTENT

Data Availability Statement

The data that support the findings of this study are available from the corresponding author upon reasonable request.

Supporting Information

The Supporting Information is available free of charge at https://pubs.acs.org/doi/10.1021/acsomega.3c10501.

Part I: Details for obtaining optimized geometrical structures: possible nitrogen-doped sites for HBC-1N samples and formation energies of all evaluated nitrogen-doped configurations, Part 2: details of orbital interactions between the nitrogen-doped and the nearest carbon atoms, Part 3: particle positions of nitrogen-doped graphene quantum dots (PDF)

■ AUTHOR INFORMATION

Corresponding Author

Minh Triet Dang − *Can Tho University, Can Tho 900000, Vietnam;* orcid.org/0000-0003-1769-4873; Email: dmtriet@ctu.edu.vn

Authors

Pham Vu Nhat − *Can Tho University, Can Tho 900000, Vietnam;* orcid.org/0000-0002-1485-6569

Nguyen Vo Anh Duy − *FPT University, Can Tho 900000, Vietnam*

Thi Nhan Tran − *Faculty of Fundamental Sciences, Hanoi University of Industry, Hanoi 100000, Vietnam*

Nguyen Thanh Si − *Institute of Environmental Science and Technology, Tra Vinh University, Tra Vinh 94000, Vietnam*

Truc Anh Nguyen − *Faculty of Mechanics, Can Tho University of Technology, Can Tho 900000, Vietnam*

Nguyen To Van − *Faculty of Chemico-Physical Engineering, Le Quy Don Technical University, Ha Noi 100000, Vietnam;* orcid.org/0000-0002-0288-5071

Nguyen Van Nghia − *Open Training Institute, Hanoi Architectural University, Hanoi 100000, Vietnam*

Peter Schall − *Van der Waals-Zeeman Institute, University of Amsterdam, Amsterdam 1098 XH, The Netherlands;* orcid.org/0000-0003-2612-2762

Van An Dinh − *Department of Precision Engineering, Graduate School of Engineering, Osaka University, Suita, Osaka 565-0871, Japan;* orcid.org/0000-0002-7290-7969

Complete contact information is available at: https://pubs.acs.org/10.1021/acsomega.3c10501

Notes

The authors declare no competing financial interest.

■ ACKNOWLEDGMENTS

This research was funded by the Vingroup Innovation Foundation (VINIF) under project code VINIF.2023.DA080. The authors acknowledge the Mississippi Center for Supercomputing Research, USA and the Information and Network Management Center at Can Tho University for providing computing resources. M.T.D. thanks Dr. Quang Huy Tran at Hanoi Pedagogical University 2 for useful discussions.

REFERENCES

(1) Shockley, W.; Queisser, H. J. Detailed Balance Limit of Efficiency of p-n Junction Solar Cells. *J. Appl. Phys.* **1961**, *32* (3), 510−519.

(2) Miller, O. D.; Yablonovitch, E.; Kurtz, S. R. Strong Internal and External Luminescence as Solar Cells Approach the Shockley−Queisser Limit. *IEEE J. Photovolt.* **2012**, *2* (3), 303−311.

(3) Ehrler, B.; Alarcón-Lladó, E.; Tabernig, S. W.; Veeken, T.; Garnett, E. C.; Polman, A. Photovoltaics Reaching for the Shockley−Queisser Limit. *ACS Energy Lett.* **2020**, *5* (9), 3029−3033.

(4) Swain, R. A.; McVey, B. F. P.; Virieux, H.; Ferrari, F.; Tison, Y.; Martinez, H.; et al. Sustainable quantum dot chemistry: effects of precursor, solvent, and surface chemistry on the synthesis of Zn3P2 nanocrystals. *Chem. Commun.* **2020**, *56* (22), 3321−3324.

(5) Goyal, A.; Demmenie, M.; Huang, C. C.; Schall, P.; Dohnalova, K. Photophysical properties of ball milled silicon nanostructures. *Faraday Discuss.* **2020**, *222*, 96−107.

(6) Roondhe, V.; Roondhe, B.; Saxena, S.; Ahuja, R.; Shukla, A. On using non-Kekulé triangular graphene quantum dots for scavenging hazardous sulfur hexafluoride components. *Heliyon* **2023**, *9* (4), No. e15388.

(7) Kumar, A.; Sayyed, M. I.; Punina, D.; Naranjo, E.; Jácome, E.; Abdulameer, M. K.; et al. Graphene quantum dots (GQD) and edge-functionalized GQDs as hole transport materials in perovskite solar cells for producing renewable energy: a DFT and TD-DFT study. *RSC Adv.* **2023**, *13* (42), 29163−29173.

(8) Pan, D.; Zhang, J.; Li, Z.; Wu, M. Hydrothermal Route for Cutting Graphene Sheets into Blue-Luminescent Graphene Quantum Dots. *Adv. Mater.* **2010**, *22* (6), 734−738.

(9) Lee, S. H.; Kim, D. Y.; Lee, J.; Lee, S. B.; Han, H.; Kim, Y. Y.; et al. Synthesis of Single-Crystalline Hexagonal Graphene Quantum Dots from Solution Chemistry. *Nano Lett.* **2019**, *19* (8), 5437−5442.

(10) Bacon, M.; Bradley, S. J.; Nann, T. Graphene Quantum Dots. *Part. Part. Syst. Charact.* **2014**, *31* (4), 415−428.

(11) Peng, J.; Gao, W.; Gupta, B. K.; Liu, Z.; Romero-Aburto, R.; Ge, L.; et al. Graphene Quantum Dots Derived from Carbon Fibers. *Nano Lett.* **2012**, *12* (2), 844−849.

(12) Dang, M. T.; Bich Thao, P. T.; Ngoc Thao, T. T.; Tien, N. T. First-principles study of electronic and optical properties of small edge-functionalized penta-graphene quantum dots. *AIP Adv.* **2022**, *12* (6), 65008.

(13) Li, X.; Rui, M.; Song, J.; Shen, Z.; Zeng, H. Carbon and Graphene Quantum Dots for Optoelectronic and Energy Devices: A Review. *Adv. Funct. Mater.* **2015**, *25* (31), 4929−4947.

(14) Li, M.; Chen, T.; Gooding, J. J.; Liu, J. Review of Carbon and Graphene Quantum Dots for Sensing. *ACS Sens.* **2019**, *4* (7), 1732−1748.

(15) Prabhu, S. A.; Kavithayeni, V.; Suganthy, R.; Geetha, K. Graphene quantum dots synthesis and energy application: a review. *Carbon Lett.* **2021**, *31* (1), 1−12.

(16) Abbas, A.; Tabish, T. A.; Bull, S. J.; Lim, T. M.; Phan, A. N. High yield synthesis of graphene quantum dots from biomass waste as a highly selective probe for Fe3+ sensing. *Sci. Rep.* **2020**, *10* (1), No. 21262.

(17) van Dam, B.; Nie, H.; Ju, B.; Marino, E.; Paulusse, J. M. J.; Schall, P.; et al. Excitation-Dependent Photoluminescence from Single-Carbon Dots. *Small* **2017**, *13* (48), No. 1702098.

(18) Feng, J.; Guo, Q.; Liu, H.; Chen, D.; Tian, Z.; Xia, F.; et al. Theoretical insights into tunable optical and electronic properties of graphene quantum dots through phosphorization. *Carbon* **2019**, *155*, 491−498.

(19) Feng, J.; Dong, H.; Pang, B.; Chen, Y.; Yu, L.; Dong, L. Tuning the electronic and optical properties of graphene quantum dots by selective boronization. *J. Mater. Chem. C* **2019**, *7* (2), 237−246.

(20) Nie, H.; Li, M.; Li, Q.; Liang, S.; Tan, Y.; Sheng, L.; et al. Carbon Dots with Continuously Tunable Full-Color Emission and Their Application in Ratiometric pH Sensing. *Chem. Mater.* **2014**, *26* (10), 3104−3112.

(21) Zhu, C.; Yang, S.; Wang, G.; Mo, R.; He, P.; Sun, J.; et al. Negative induction effect of graphite N on graphene quantum dots: tunable band gap photoluminescence. *J. Mater. Chem. C* **2015**, *3* (34), 8810−8816.

(22) Gómez, I. J.; Vázquez Sulleiro, M.; Dolečková, A.; Pizúrová, N.; Medalová, J.; Roy, R.; et al. Exploring the Emission Pathways in Nitrogen-Doped Graphene Quantum Dots for Bioimaging. *J. Phys. Chem. C* **2021**, *125* (38), 21044−21054.

(23) Vorontsov, A. V.; Tretyakov, E. V. Determination of graphene's edge energy using hexagonal graphene quantum dots and PM7 method. *Phys. Chem. Chem. Phys.* **2018**, *20* (21), 14740−1452.

(24) Hafner, J. Ab-initio simulations of materials using VASP: Density-functional theory and beyond. *J. Comput. Chem.* **2008**, *29* (13), 2044−2078.

(25) Aliano, A.; Cicero, G. Ab Initio DFT Simulations of Nanostructures. In *Encyclopedia of Nanotechnology*; Bhushan, B., Ed.; Springer Netherlands: Dordrecht, 2012; pp 11−17.

(26) Nhat, P. V.; Si, N. T.; Tram, N. T. T.; Duong, L. Van.; Nguyen, M. T. Elucidating the binding mechanism of thione-containing mercaptopurine and thioguanine drugs to small gold clusters. *J. Comput. Chem.* **2020**, *41* (19), 1748−1758.

(27) Si, N. T.; Nhung, N. T. A.; Bui, T. Q.; Nguyen, M. T.; Nhat, P. V. Gold nanoclusters as prospective carriers and detectors of pramipexole. *RSC Adv.* **2021**, *11* (27), 16619−16632.

(28) Ta, L. T.; Hamada, I.; Morikawa, Y.; Dinh, V. A. Adsorption of toxic gases on borophene: surface deformation links to chemisorptions. *RSC Adv.* **2021**, *11* (30), 18279−18287.

(29) Nguyen-Tran, T.; Dinh, V. A.; Van Ly, N.; Luong, H. D.; Pham, D. T.; Truong, T. T.; et al. Novel (110) Double-Layered Guanidinium-Lead Iodide Perovskite Material: Crystal Structure, Electronic Structure, and Broad Luminescence. *J. Phys. Chem. C* **2021**, *125* (1), 964−972.

(30) Frisch, M. J.; Trucks, G. W.; Schlegel, H. B.; Scuseria, G. E.; Robb, M. A.; Cheeseman, J. R.;et al. *Gaussian 16*, revision B.01; Gaussian Inc.: Wallingford, CT, 2016.

(31) Liao, X.; Lu, R.; Xia, L.; Liu, Q.; Wang, H.; Zhao, K.; et al. Density Functional Theory for Electrocatalysis. *Energy Environ. Mater.* **2022**, *5* (1), 157−185.

(32) Iikura, H.; Tsuneda, T.; Yanai, T.; Hirao, K. A long-range correction scheme for generalized-gradient-approximation exchange functionals. *J. Chem. Phys.* **2001**, *115* (8), 3540−3544.

(33) Tsuneda, T.; Hirao, K. Long-range correction for density functional theory. *Wiley Interdiscip. Rev.: Comput. Mol. Sci.* **2014**, *4* (4), 375−390.

(34) Lee, C.; Yang, W.; Parr, R. G. Development of the Colle-Salvetti correlation-energy formula into a functional of the electron density. *Phys. Rev. B* **1988**, *37* (2), 785−789.

(35) Zhao, Y.; Truhlar, D. G. The M06 suite of density functionals for main group thermochemistry, thermochemical kinetics, noncovalent interactions, excited states, and transition elements: two new functionals and systematic testing of four M06-class functionals and 12 other functionals. *Theor. Chem. Acc.* **2008**, *120* (1), 215−241.

(36) Perdew, J. P.; Burke, K.; Ernzerhof, M. Generalized Gradient Approximation Made Simple. *Phys. Rev. Lett.* **1996**, *77* (18), 3865−3868.

(37) Tsuneda, T. Theoretical investigations on geometrical and electronic structures of silver clusters. *J. Comput. Chem.* **2019**, *40* (1), 206−211.

(38) O'boyle, N. M.; Tenderholt, A. L.; Langner, K. M. cclib: A library for package-independent computational chemistry algorithms. *J. Comput. Chem.* **2008**, *29* (5), 839−845.

(39) Ni, Z.; Jia, H.; Pi, X.; Yang, D. Density functional theory study on the boron and phosphorus doping of germanium quantum dots. *RSC Adv.* **2017**, *7* (80), 50935−50941.

(40) Ochterski, J. W. *Thermochemistry in Gaussian*; Gaussian Inc., 2000.

(41) Kaur, M.; Kaur, M.; Sharma, V. K. Nitrogen-doped graphene and graphene quantum dots: A review on synthesis and applications

https://doi.org/10.1021/acsomega.3c10501
ACS Omega 2024, 9, 20056−20065

in energy, sensors and environment. *Adv. Colloid Interface Sci.* **2018**, *259*, 44−64.
(42) Liu, R.; Wu, D.; Feng, X.; Müllen, K. Bottom-Up Fabrication of Photoluminescent Graphene Quantum Dots with Uniform Morphology. *J. Am. Chem. Soc.* **2011**, *133* (39), 15221.
(43) Chandler, D. *Introduction to Modern Statistical Mechanics*; Oxford University Press, 1987.
(44) Tönshoff, C.; Müller, M.; Kar, T.; Latteyer, F.; Chassé, T.; Eichele, K.; Bettinger, H. F. B3N3 Borazine Substitution in Hexa-peri-Hexabenzocoronene: Computational Analysis and Scholl Reaction of Hexaphenylborazine. *ChemPhysChem* **2012**, *13* (5), 1173−1181.
(45) Hudgins, D. M.; Sandford, S. A. Infrared Spectroscopy of Matrix Isolated Polycyclic Aromatic Hydrocarbons. 2. PAHs Containing Five or More Rings. *J. Phys. Chem. A* **1998**, *102* (2), 344−352.
(46) Xu, X.; Gao, F.; Bai, X.; Liu, F.; Kong, W.; Li, M. Tuning the Photoluminescence of Graphene Quantum Dots by Photochemical Doping with Nitrogen. *Materials* **2017**, *10* (11), No. 1328.
(47) Kaltsoyannis, N.; McGrady, J. E. *Principles and Applications of Density Functional Theory in Inorganic Chemistry II*; Springer-Verlag: Berlin, Heidelberg, 2004.
(48) Peverati, R.; Truhlar, D. G. Screened-exchange density functionals with broad accuracy for chemistry and solid-state physics. *Phys. Chem. Chem. Phys.* **2012**, *14* (47), 16187−16191.
(49) Tsuneda, T.; Singh, R. K.; Nakata, A. On low-lying excited states of extended nanographenes. *J. Comput. Chem.* **2017**, *38* (23), 2020−2029.
(50) Nhat, P. V.; Si, N. T.; Nguyen, M. T. Structural Evolution and Stability Trend of Small-Sized Gold Clusters Aun (n = 20−30). *J. Phys. Chem. A* **2020**, *124* (7), 1289−1299.
(51) Ye, R.; Peng, Z.; Metzger, A.; Lin, J.; Mann, J. A.; Huang, K.; et al. Bandgap Engineering of Coal-Derived Graphene Quantum Dots. *ACS Appl. Mater. Interfaces* **2015**, *7* (12), 7041−7048.

https://doi.org/10.1021/acsomega.3c10501
ACS Omega 2024, 9, 20056−20065